Bio-Inspired Computer Fovea Model Based on Hexagonal-Type Cellular Neural Network

Chao-Hui Huang, *Student Member, IEEE*, and Chin-Teng Lin, *Fellow, IEEE*

***Abstract*—For decades, numerous scientists have examined the following questions: "How do humans see the world?" and "How do humans experience vision?" To answer these questions, this study proposes a computer fovea model based on hexagonal-type cellular neural network (hCNN). Certain biological mechanisms of a retina can be simulated using an in-state-of-art architecture named CNN. Those biological mechanisms include the behaviors of the photoreceptors, horizontal cells, ganglions, and bipolar cells, and their co-operations in the retina. Through investigating the model and the abilities of the CNN, various properties of the human vision system can be simulated. The human visual system possesses numerous interesting properties, which provide natural methods of enhancing visual information. Various visual information enhancing algorithms can be developed using these properties and the proposed model. The proposed algorithms include color constancy, image sharpness, and some others. This study also discusses how the proposed model works for video enhancement and demonstrates it experimentally.**

***Index Terms*—Bipolar cell, cellular neural networks (CNNs), color constancy, fovea, ganglion, hexagonal, horizontal cell, photoreceptor, retina, sharpness.**

I. Introduction

AS A HIGHLY structured neuron network, a retina extracts and processes the stimulation from an image projected upon it by the optical system of the eye [1]–[3]. This process is extremely complex. Consequently, analyzing, modeling, and even simulating the retina have been considered highly challenging tasks. To meet these challenges, numerous studies have been published during the past decade: for example, Shah *et al.* studied the information processing procedure of the retina in both the space and time domains [4]. Based on the study of Shah *et al.*, Thiem later proposed a bio-inspired retina model capable of implementing some visual properties in the human vision system [5]. Roska and Bálya *et al.* even discussed the parallel structure of retina and proposed an implementation on cellular neural networks (CNNs) [6]. Their study demonstrated that certain visual information enhancing mechanisms exist in the human vision system. Accordingly, this study focuses on how to simulate the retinal fovea based on hexagonal-type CNN (hCNN). Furthermore, this study examines how to improve images and videos based on the proposed computer fovea model.

First, the biological structure of a retina must be understood. Five major types of neurons exist in the five layers of the retina. Outer nuclear layer contains photoreceptors, Inner nuclear layer contains horizontal cells, amacrine cells and bipolar cells, and ganglion layer contains ganglions. Moreover, the outer plexiform layer contains the synapse connections among the photoreceptors, the horizontal cells and the bipolar cells. Finally, inner plexiform layer contains the synapse connections among the bipolar cells, the amacrine cells and the ganglions [1], [7].

The human visual system contains four kinds of photoreceptor: L-cone, M-cone, S-cone, and rod cells. These different types of photoreceptors react to different wavelengths of light (Fig. 1). Rod cells can sense light intensity, while L-cone, M-cone, S-cone cells can detect color information. Sometimes the cooperation of these cone cells can also detect the light intensity. We are already aware that the ganglion is usually activated by a set of the photoreceptors via other bipolar, horizontal, and other types of cells [2], [8]. This set contains several varieties of photoreceptors. The differences among those different types of photoreceptors results in the variation among the ganglions. The two main types of ganglions are center-on/surround-off and center-off/surround-on. Fig. 2 illustrates two examples, where Fig. 2(a) shows an example of center-surround ganglion. The center of a group of photoreceptors reacts to the stimulation differently to the peripheral part of the group. The ganglions can generally be classified as red-green (RG) ganglion, blue-yellow (BY) ganglion, and black-white (BW) ganglion [see Fig. 2(b) and (c)] and others [1]. Furthermore, based on the different responses of neighboring ganglions, the visual information can be sensed. The visual information included luminance and color. Fig. 3 shows the ganglions' response to the light simulation. Fig. 3 (a) represents how the center-green-on/surround-red-off ganglions respond on the border of the red and green region. Fig. 3 (b)–(d) shows the responses of the different kinds of ganglions.

The ganglion is important in the human vision system and processes most visual information. Visual information includes light intensity and color information. The mechanism which is used to process this visual information in the human vision system is so-called early vision system, also known as the preattentive vision system. The early vision system represents a set of the first stage information processing mechanisms of visual processing. Those mechanisms are operated in parallel across

Manuscript received January 5, 2006; revised September 17, 2006. This work was supported in part by the National Science Council, Taiwan, under Grant 95-2752-E-009-011-PAE, Ministry of Economic Affairs, Taiwan, under Grant 95-EC-17-A-02-S1-032, and MOE ATU Program 95W803E. This paper was recommended by Guest Editor O. Yadid-Pecht.

C.-H. Huang is with the Department of Electrical and Control Engineering, National Chiao-Tung University (NCTU), Hsinchu 300, Taiwan, R.O.C. (e-mail: chhuang.ece90g@nctu.edu.tw).

C.-T. Lin is with the Department of Electrical and Control Engineering and the Department of Computer Science and the Brain Research Center, National Chiao-Tung University (NCTU), Hsinchu 300, Taiwan, R.O.C. (e-mail: ctlin@mail.nctu.edu.tw).

Digital Object Identifier 10.1109/TCSI.2006.887975

1057-7122/$25.00 © 2007 IEEE

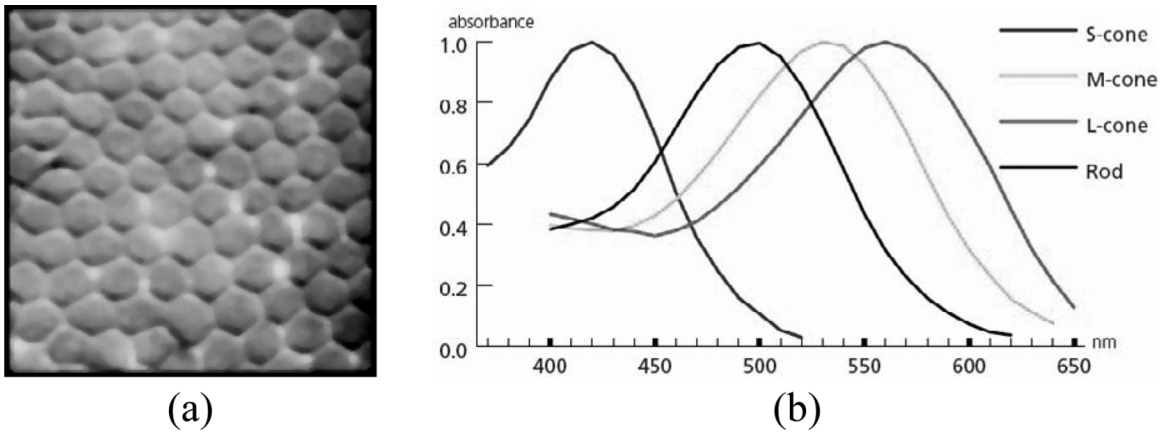

Fig. 1. Biological structure of the photoreceptors in the fovea of a mammalian. (a) Photoreceptor group in a fovea. (b) Photoreceptors can be classified according to the stimulation they react to [1].

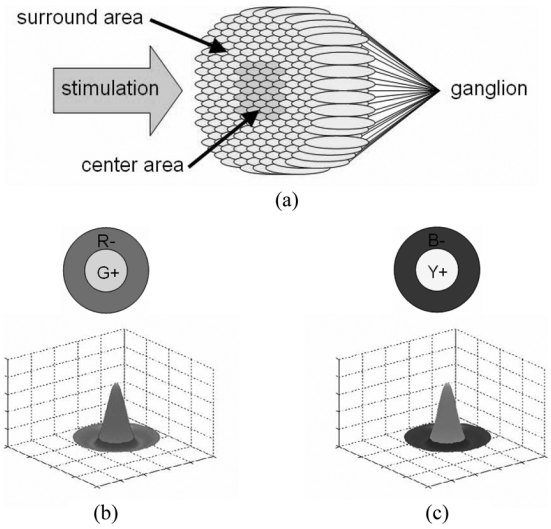

Fig. 2. Example of a ganglion. (a) A ganglion collects information from a set of neighboring photoreceptors. The response of the central part of the set differs from that of the peripheral part of the set. Based on the difference between the types of photoreceptor, ganglion can be classified into RG, BY, and BW types. (b) The RF of a center-green-on/surround-red-off ganglion. (c) The RF of a center-yellow-on/surround-blue-off ganglion.

the visual field, and are believed to be used for detecting certain fundamental visual features [1].

According to Jain *et al.*, the human vision system possesses two fundamental features: first, in some respects the retina acts like a low-pass filter. Generally, the result of the low-pass filtering represents an average intensity of light for a specific local area. The result of this operation is termed "the first-order feature." Second, a difference exists between the intensity of the external light and that projected into the retina. According to some studies, the boundary detection operation in the human vision system is based on this kind of feature, and is related to the zero crossing of a Laplacian of two Gaussians (LoG). Sometimes the result of this operation is called "the second-order feature [9]."

The mechanisms of information processing in the retina are rather complex and remain unclear. This study thus mainly aims to design and approximate the receptive fields (RFs) of the cells on a retinal fovea. From the signal processing perspective, the RFs can be referred to as a finite impulse response of a spatial filter [4], [8], [10]. In this investigation, the well-known CNN is used to realize the spatial filter.

CNN represents the next generation of computational architecture. Similar to a biological system, each cell in the CNN can communicate only with its immediate neighborhood. Consequently, using the CNN to implement the proposed model makes sense. According to some previous studies, hexagonal image processing (HIP) is much reasonable for image processing, particularly for bio-inspired models (refer to Fig. 1) [11]–[15]. Thus, this study suggests a special type of CNN)—the hCNN. Furthermore, hCNN provides a means of reducing implementation problems without increasing the complexity [12].

Based on the biological investigations and the abilities of the CNN, this work proposes an hCNN-based computer fovea model. The proposed model simulates certain biological mechanisms of the retina and the fovea, including the photoreceptors, bipolar cells, horizontal cells, ganglions, and the co-operations of those cells in a fovea and a retina. Consequently, some properties of the human vision system can be simulated. The human vision system possesses various interesting properties. Some of those properties can even be used to enhance the visual information. This study also presents how these properties provide visual enhancement.

This study first briefly introduces the hCNN, and also discusses the stable central linear system for the hCNN and develops its implementations. Those implementations are required for the proposed model, including CNN-based Laplace-like operators, CNN-based Gaussian-like operators and their inverse operators. Subsequently, the CNN-based computer fovea model is introduced. Building on the above, several experiments are presented, including vision enhancing algorithms based on this model. Finally, conclusions are drawn.

II. Method and Methodology

A. hCNNs

The CNN has already been shown to be a very powerful image processing kernel with artificial-intelligent-like abilities

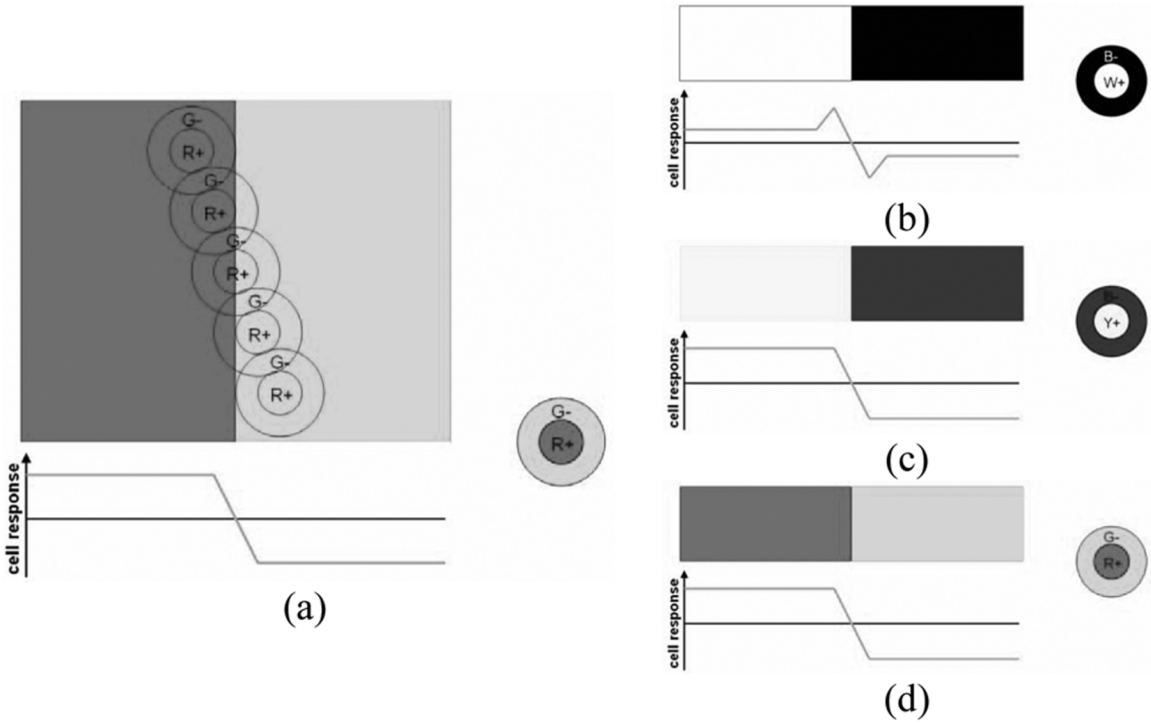

Fig. 3. Based on the different responses of neighboring ganglions, the visual information can be sensed. The visual information included luminance and color. (a) The center-green-on/surround-red-off ganglions respond on the border of red and green region. (b)–(d) Responses of the different kinds of ganglions. [1].

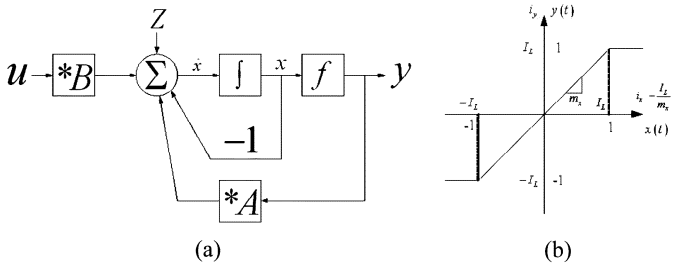

Fig. 4. Architecture of CNN is shown in (a), and along with the dynamic route of state in CNN.

[16], [17]. Since Chua and Yang first introduced CNN, it has been widely applied in numerous areas. CNN offers an alternative to a fully connected neural network, and has evolved into a paradigm for this type of array. As shown in Fig. 4(a), the dynamic equation of the CNN can be represented by the following:

$$\dot{x}_t(i,j) = -x_t(i,j) + \sum_{k,l\in N_r(i,j)} A(i,j;k,l)\, y_t(k,l) + \sum_{k,l\in N_r(i,j)} B(i,j;k,l)\, u(k,l) + I \quad (1)$$

where

$$y_t = f(x_t) = \frac{1}{2}\left(|x_t+1| - |x_t-1|\right). \quad (2)$$

Here (2) can be represented as Fig. 4(b).

1) CNNs for HIP: The CNN is particularly considered as an image processor in many areas. Given its flexibility and other abilities, CNN provides excellent computational performance. One area of flexibility is that CNN can be used as a parallel and symmetric structure neural network. Usually, the CNN are eight-connected structured network. In the fact, CNN is **not only** being constructed as eight-connected. If we construct the CNN on a flat plane, the cells can be connected as many kinds of symmetric structure [18]. One possible structure is the six-connected structure, or as the well-known, the hexagonal-type structure [12].

An hCNN can be described by [12]

$$\frac{d}{dt}x_t(\mathbf{i}) = -x_t(\mathbf{i}) + \sum_{\mathbf{j}\in N(\mathbf{i})} A(\mathbf{i}-\mathbf{j})\, y_t(\mathbf{j}) + \sum_{\mathbf{j}\in N(\mathbf{i})} B(\mathbf{i}-\mathbf{j})\, u(\mathbf{j}) + I \quad (3)$$

where

$$y_t = f(x_t) = \frac{1}{2}\left(|x_t+1| - |x_t-1|\right). \quad (4)$$

To be consistent with 1-D, 2-D rectangular, and 2-D hexagonal systems, the index is represented using bold characters in this study). Meanwhile, for convenience, this study uses the following mathematical symbols to present the templates in the hCNN

$$A = \left\langle \begin{matrix} & a_3 & \\ a_4 & & a_0 \\ & a_5 & \end{matrix} \right\rangle \quad \left\langle \begin{matrix} & a_2 & \\ & & a_1 \\ & a_6 & \end{matrix} \right\rangle$$
$$B = \left\langle \begin{matrix} & b_3 & \\ b_4 & & b_0 \\ & b_5 & \end{matrix} \right\rangle \quad \left\langle \begin{matrix} & b_2 & \\ & & b_1 \\ & b_6 & \end{matrix} \right\rangle$$
$$I = z \quad (5)$$

where A denotes the feedback template, B represents the control template, and I is the bias. Notably, the indexes in the tem-

plates are the same as HIP designed by Middleton for realizing the hexagonal Fourier transform where necessary [19].

2) Stable Central Linear Systems and Their Inverse Systems: If the CNN is considered as an image processor then numerous linear properties must be analyzed; for example, the states located in the non-saturated region. Crounse and Chua mentioned how to analyze the CNN-based image processing in the frequency domain [20]. A similar mechanism can be applied to the hCNN [12]. Assuming all of the cells operate in the linear region, that is, $|x_{\mathbf{i}}| < 1$, then $y_{\mathbf{i}} = x_{\mathbf{i}}$. Thus, (3) can be reformulated as

$$\frac{d}{dt}x_t(\mathbf{i}) = -x_t(\mathbf{i}) + \sum_{\mathbf{j}\in N(\mathbf{i})} A(\mathbf{i}-\mathbf{j})\,x_t(\mathbf{j}) + \sum_{\mathbf{j}\in N(\mathbf{i})} B(\mathbf{i}-\mathbf{j})\,u(\mathbf{j}) + I. \quad (6)$$

Let $a_{\mathbf{n}} \in A$, the linearized templates then can be represented by [20]

$$a_{\mathbf{n}} = \begin{cases} A_{\mathbf{n}} - 1, & \mathbf{n} = 0 \\ A_{\mathbf{n}}, & \mathbf{n} \in N_r(\mathbf{i}) \\ 0, & \text{otherwise.} \end{cases} \text{ and } \begin{cases} B_{\mathbf{n}}, & (\mathbf{n}) \in N_r(\mathbf{i}) \\ 0, & \text{otherwise.} \end{cases} \quad (7)$$

The dynamics can then be represented in a convoluted form as

$$\frac{d}{dt}x_t(\mathbf{n}) = a(\mathbf{n}) \otimes x_t(\mathbf{n}) + b(\mathbf{n}) \otimes u(\mathbf{n}) + I \quad (8)$$

where $\otimes$ represents a hexagonal convolution.

The dynamics can be written into [21]

$$\frac{d}{dt}\tilde{X}_t(\mathbf{w}) = \tilde{A}(\mathbf{w})\,\tilde{X}(\mathbf{w}) + \tilde{B}(\mathbf{w})\tilde{U}(\mathbf{w}) + I\delta(\mathbf{w}) \quad (9)$$

if and only if all of the discrete hexagonal Fourier transforms exist. Regarding the dynamics, assume that infinite time is available and that a discrete hexagonal Fourier transform exists for all $\mathbf{w}$, then (8) can be represented as follows [20]:

$$\tilde{X}_\infty(\mathbf{w}) = \tilde{H}(\mathbf{w})\tilde{U}(\mathbf{w}) \quad (10)$$

where

$$\tilde{H}(\mathbf{n}) \triangleq \frac{-\tilde{B}(\mathbf{n})}{\tilde{A}(\mathbf{n})}. \quad (11)$$

It is already known that if $\tilde{A}(\mathbf{w}) < 0$ for all $\mathbf{w}$, then the central linear system will be stable. Thus, the equilibrium state can be thought of as a version of the input that has been spatially filtered by the hexagonal transfer function $\tilde{H}(\mathbf{w})$ [22].

Based on the above, this study develops some operators that are required by the proposed model. These operators include CNN-based Laplace-like operators, CNN-based Gaussian-like operators and their inverse operators. These operators are introduced in Sections II-A-II-A–B.

CNN-Based Laplace-Like Operator: A Laplace operator can be represented as

$$l_r(\mathbf{n}) = \begin{bmatrix} 0 & -1 & 0 \\ -1 & 4 & -1 \\ 0 & -1 & 0 \end{bmatrix}. \quad (12)$$

The zero-frequency component of the Fourier transform of (12) is zero. This fact implies the inverse operation of (12) is difficult in the discrete environment. Thus, a small positive value ε^2 is added to (12). Accordingly, the Laplace-like operator is as follows:

$$l_r(\mathbf{n}) = \begin{bmatrix} 0 & -1 & 0 \\ -1 & 4+\varepsilon^2 & -1 \\ 0 & -1 & 0 \end{bmatrix}. \quad (13)$$

Notably, the value of ε approaches zero as $l_r(\mathbf{n})$ approaches a Laplace operator. For HIP, the Laplace-like operator is

$$l_h(\mathbf{k}) = \left\langle \begin{array}{ccccc} & & -1 & -1 & \\ -1 & & 6+\varepsilon^2 & & -1 \\ & & -1 & -1 & \end{array} \right\rangle. \quad (14)$$

If and only if the Fourier transform of the Laplace-like operator $l(\mathbf{n})$ exists and is denoted as

$$\mathcal{F}_{\mathbf{w}}\{l(\mathbf{n})\} \triangleq \tilde{L}(\mathbf{w}). \quad (15)$$

Next, map (15) into (11). Since $\tilde{A}(\mathbf{w}) < 0$ for all $\mathbf{w}$ are required, we choose $\tilde{A}(\mathbf{w}) = -1$. Thus,

$$\frac{-\tilde{B}(\mathbf{w})}{\tilde{A}(\mathbf{w})} = \tilde{L}(\mathbf{w}) = \frac{-\tilde{L}(\mathbf{w})}{-1}. \quad (16)$$

According to (7), the coefficients of the system that has been described in (16) can be represented as

$$a(\mathbf{n}) = -\delta(\mathbf{n}) \text{ and } b(\mathbf{n}) = l(\mathbf{n}). \quad (17)$$

Thus, the templates are given by $A = a(\mathbf{n}) + \delta(\mathbf{n})$, and $B = b(\mathbf{n})$, where $\delta(\cdot)$ represents *Dirac Delta function*. Finally, for the CNN-based Laplace-like operator, the templates are as follows:

$$A_r = \begin{bmatrix} 0 & 0 & 0 \\ 0 & 0 & 0 \\ 0 & 0 & 0 \end{bmatrix} \text{ and } B_r = \begin{bmatrix} 0 & -1 & 0 \\ -1 & 4+\varepsilon^2 & -1 \\ 0 & -1 & 0 \end{bmatrix}. \quad (18)$$

Meanwhile, for the HIP, the templates are

$$A_h = \left\langle \begin{array}{ccccc} & & 0 & & \\ & 0 & & 0 & \\ 0 & & 0 & & 0 \end{array} \right\rangle$$

$$B_h = \left\langle \begin{array}{ccccc} & & -1 & -1 & \\ -1 & & 6+\varepsilon^2 & & -1 \\ & & -1 & -1 & \end{array} \right\rangle. \quad (19)$$

For convenience, this study denotes the CNN-based Laplace-like operator as follows:

$$\mathrm{CNN}_{\mathrm{Laplace},\varepsilon}(u(\mathbf{k})) \quad (20)$$

where $u(\mathbf{k})$ denotes the input, ε is a corresponding parameter, and the initial state of all cells is zero.

In fact, for any CNN, if the initial condition x_0, the template A, and the bias I are zero, then the system is simply a FIR

system and the template B can be considered as the FIR operator.

For the inverse Laplace-like operator, the inverse system of (16) can be used. That is

$$\frac{-\tilde{B}(\mathbf{w})}{\tilde{A}(\mathbf{w})} = \tilde{L}^{-1}(\mathbf{w}) = \frac{-1}{-\tilde{L}(\mathbf{w})}. \tag{21}$$

Notably, since the condition, $\tilde{A}(\mathbf{w}) < 0$ for all $\mathbf{w}$ must be satisfied, this study sets $\tilde{A}(\mathbf{w}) = -\tilde{L}(\mathbf{w})$. Thus, the templates can be obtained as follows:

$$A_r = \begin{bmatrix} 0 & 1 & 0 \\ 1 & -\left(3+\varepsilon^2\right) & 1 \\ 0 & 1 & 0 \end{bmatrix} \text{ and } B_r = \begin{bmatrix} 0 & 0 & 0 \\ 0 & 1 & 0 \\ 0 & 0 & 0 \end{bmatrix}. \tag{22}$$

For HIP, the templates are

$$A_h = \left\langle \begin{matrix} & 1 & \\ 1 & -\left(5+\lambda^2\right) & 1 \\ & 1 & \end{matrix} \right\rangle$$
$$B_h = \left\langle \begin{matrix} & 0 & \\ 0 & 1 & 0 \\ & 0 & \end{matrix} \right\rangle. \tag{23}$$

For convenience, the CNN-based Inverse Laplace-like Operator is denoted here as follows:

$$\mathrm{CNN}^{-1}_{\mathrm{Laplace},\varepsilon}(u(\mathbf{k})) \tag{24}$$

where $u(\mathbf{k})$ denotes the input, and ε represents the corresponding parameter in (18) and (19). The initial condition x_0 and the bias I are zero.

CNN-Based Gaussian-Like Operator: Kobayashi *et al.* suggested an active resister network for Gaussian-like filtering for the image [20]. The proposed system can be described as follows [13], [22]:

$$h(\mathbf{n}) = \frac{v(\mathbf{n})}{u(\mathbf{n})} \tag{25}$$
$$\text{where } u(\mathbf{n}) = \begin{bmatrix} 1 & -\left(2+\lambda^2\right) & 1 \end{bmatrix}$$
$$v(\mathbf{n}) = \begin{bmatrix} 0 & -\lambda^2 & 0 \end{bmatrix}. \tag{26}$$

The Fourier transforms are denoted as $F_{\mathbf{w}}\{u(\mathbf{n})\} \triangleq \tilde{U}(\mathbf{w})$, and $F_{\mathbf{w}}\{v(\mathbf{n})\} \triangleq \tilde{V}(\mathbf{w})$, then the system can be described as

$$\tilde{H}(\mathbf{w}) \triangleq \frac{-\tilde{B}(\mathbf{w})}{\tilde{A}(\mathbf{w})} = \frac{\tilde{V}(\mathbf{w})}{\tilde{U}(\mathbf{w})}. \tag{27}$$

Thus, the templates can be obtained by

$$A = u(\mathbf{n}) + \delta(\mathbf{n}) \text{ and } B = -v(\mathbf{n}). \tag{28}$$

The templates for different architectures are listed below.

1-D CNN:

$$A = \begin{bmatrix} 1 & -\left(1+\lambda^2\right) & 1 \end{bmatrix} \text{and } B = \begin{bmatrix} 0 & \lambda^2 & 0 \end{bmatrix} \tag{29}$$

2-D Rectangular-type CNN:

$$A_r = \begin{bmatrix} 0 & 1 & 0 \\ 1 & -\left(3+\lambda^2\right) & 1 \\ 0 & 1 & 0 \end{bmatrix} \text{ and } B_r = \begin{bmatrix} 0 & 0 & 0 \\ 0 & \lambda^2 & 0 \\ 0 & 0 & 0 \end{bmatrix}. \tag{30}$$

2-D hCNN:

$$A_h = \left\langle \begin{matrix} & 1 & \\ 1 & -\left(5+\lambda^2\right) & 1 \\ & 1 & \end{matrix} \right\rangle$$
$$B_h = \left\langle \begin{matrix} & 0 & \\ 0 & \lambda^2 & 0 \\ & 0 & \end{matrix} \right\rangle. \tag{31}$$

Shi proposed a CNN-based Gabor-type filtering model based on the study of Kobayashi [22]. His model is based on a Gaussian-like operator similar to (30) However, Shi modified the dynamic equation of the CNN to reduce the complexity of the hardware implementation. The proposed model requires no such modification.

For convenience, this study denotes the CNN-based Gaussian-like operator as follows:

$$\mathrm{CNN}_{\mathrm{Gaussian},\lambda}(u(\mathbf{k})) \tag{32}$$

where $u(\mathbf{k})$ is the input, λ is the corresponding parameter, and the initial condition x_0 and the bias I are zero.

For the inverse Gaussian-like operator, we have

$$\tilde{H}(\mathbf{w}) \triangleq \frac{-\tilde{B}(\mathbf{w})}{\tilde{A}(\mathbf{w})} = \frac{\tilde{U}(\mathbf{w})}{\tilde{V}(\mathbf{w})}. \tag{33}$$

Since the condition $\tilde{V}(\mathbf{w}) < 0$ for all $\mathbf{w}$ must be met, it is concluded that $\tilde{B}(\mathbf{w}) = -\tilde{U}(\mathbf{w})$. The templates can be obtained from $A = v(\mathbf{n}) + \delta(\mathbf{n})$ and $B = -u(\mathbf{n})$.

The CNN-based inverse Gaussian-like operators for different architectures are listed as follows.

1-D CNN:

$$A' = \begin{bmatrix} 0 & -\lambda^2+1 & 0 \end{bmatrix} \text{and } B' = -\begin{bmatrix} 1 & -\left(2+\lambda^2\right) & 1 \end{bmatrix}. \tag{34}$$

2-D Rectangular-type CNN:

$$A'_r = \begin{bmatrix} 0 & 0 & 0 \\ 0 & -\lambda^2+1 & 0 \\ 0 & 0 & 0 \end{bmatrix}$$
$$B'_r = -\begin{bmatrix} 0 & 1 & 0 \\ 1 & -\left(4+\lambda^2\right) & 1 \\ 0 & 1 & 0 \end{bmatrix}. \tag{35}$$

2-D hCNN:

$$A'_h = \begin{bmatrix} & 0 & \\ 0 & -\lambda^2+1 & 0 \\ & 0 & \end{bmatrix}$$
$$B'_h = \begin{bmatrix} & 1 & \\ 1 & -(6+\lambda^2) & 1 \\ & 1 & \end{bmatrix}. \quad (36)$$

Finally, a CNN-based inverse Gaussian-like operator can be denoted as

$$\mathrm{CNN}^{-1}_{\mathrm{Gaussian},\lambda}(u(\mathbf{k})) \quad (37)$$

where $u(\mathbf{k})$ denotes the input, λ represents the degree of Gaussian function and the initial condition x_0 and the bias I are zero.

B. Computer Fovea Model

Since a retina is a highly structured network of neurons, it has become a valuable research topic in the field of human computer interaction (HCI). Many studies have studied the structure of the retina and the biological evidence regarding the functions of the human vision system [23], [24]. Notably, some researchers have even analyzed visual information processing in the retina [4], [8]. Building on these previous works, this study constructs] a new computer fovea model.

The retinal fovea is located at the center of the retina, and is the region with the highest visual acuity. The fovea is a 0.2–0.4 mm diameter rod-free area with very thin, densely packed photoreceptors. The photoreceptors in the fovea are arranged in a roughly hexagonal pattern [see Fig. 1(a)] [3], and the average cone spacing (csp) has been estimated at around 2.5 to 2.8 μm, where has been considered as the most important area in a retina. The retinal fovea is directed towards the desired object of study. The retinal fovea almost exclusively contains high density cones.

Fig. 5 shows the proposed hCNN-based computer fovea model, where Fig. 5(a) illustrates the top-view of the computer fovea. The computer fovea is constructed using a set of photoreceptors, which are hexagonally arranged [see Fig. 5(b)]. Fig. 5(c) is the signal processing system of the cells in the fovea model. Thiem mentioned that because there are direct synaptic connections between bipolar cell and the ganglion, and only few influences by the amacrin cell in the fovea. Hence, in his research, he suggested that the bipolar cell and the amacrin cell are neglected [5]. However, the horizontal cells are already known to exist and connect directly to the bipolar cells [8]. Thus, this study suggests keeping the bipolar cell and the ganglion in the system, and considering the ganglion as a direct synaptic connection.

A simplified version of the proposed model is required to obtain the parameters of the proposed architecture. The simplified version of the proposed model ignores the differences between the L-cone, the M-cone, and the S-cone cells. Restated, the system considered for obtaining the parameters is assumed

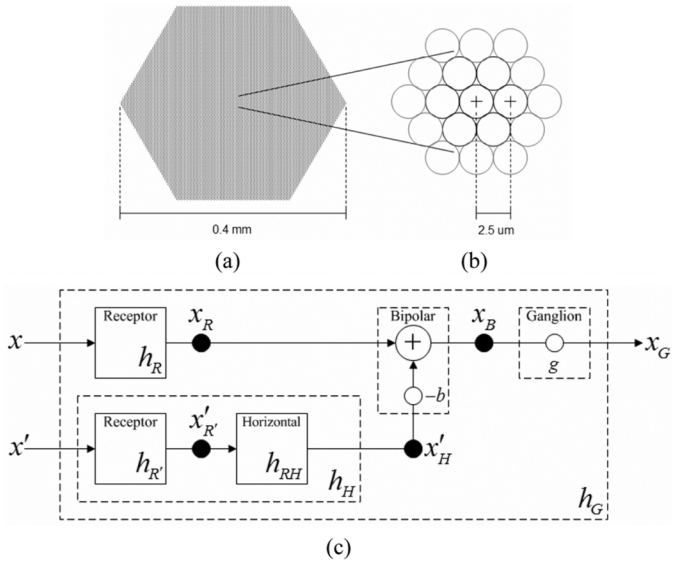

Fig. 5. Proposed computer fovea model. (a) Computer fovea which has been constructed using hexagonally arranged cells. The width of the computer fovea is approximately 0.4 mm, and is 161 csp. (b) Part of the computer fovea and illustrates the arrangement of the photoreceptors. The diameter of the photoreceptor is approximately 2.5 um. (c) Signal processing system of each cell in the fovea model. The input x is the input signal of the center area, while x' is the input signal of the surrounding area. For a monotonic input signal, x equals x'.

to be monochromatic. Thus, $x'_{R'}$ equals x_R. Sections II-B-1)–3), discuss behavioral variation among the cone cells.

1) Ganglion: The ganglions of the mammalian retina have been characterized into X-, Y-, and W-types based on the spatiotemporal distribution of the excitation and inhibition. The cells are classified according to their latency from the optic chiasm stimulations [8]. The X-type ganglions behave linearly in both the space and time domain and also provide the best spatial resolution, but the most ganglions are considered direct synapse connections. Consequently, in this study, the ganglion has been considered as an amplifier which contains a bias g.

Based on the above, $h_G(\mathbf{k})$ can take the form

$$h_G(\mathbf{k}) = g \cdot h_B(\mathbf{k}) = g \cdot h_{RB}(\mathbf{k}) \otimes h_R(\mathbf{k})$$
$$= g \cdot (\delta(\mathbf{k}) - b \cdot h_{RH}(\mathbf{k})) \otimes h_R(\mathbf{k}). \quad (38)$$

Some physiological experiments indicated that the RF of the ganglion exhibits a center/surround characteristic. Furthermore, Thiem stated that the RF of ganglions can be modeled as follows [5]:

$$h_G(\mathbf{k}) = \Delta(g_{\sigma_G}(\mathbf{k})) \quad (39)$$

where $\Delta(\cdot)$ represents the Laplace operator, and $g_{\sigma_G}(\cdot)$ is a Gaussian function. According to Hubel, under the optimum lighting condition, the central part of RF is about 10 μm (4 csp) [1]. Thus, Thiem also recommends a standard deviation of $\sigma_G = (5\ \mu\mathrm{m}/\sqrt{2}) = \sqrt{2}$ (csp) [5].

A combination of the CNN-based Laplace-like operator and the CNN-based Gaussian-like operator can be employed to derive the $h_G(\mathbf{k})$. That is

$$h_G(\mathbf{k}) = \mathrm{CNN}_{\mathrm{Laplace},\varepsilon}(\mathrm{CNN}_{\mathrm{Gaussian},\lambda_G}(\mathbf{k})) \quad (40)$$

TABLE I
CORRESPONDING IN (42) FOR DEVIATION IN (41)

σ in Eq.(42)	Corresponding λ in Eq. (42)	MSE
$\sqrt{2}$	~0.567700	3.5783×10^{-5}
1.5	~0.536040	2.8497×10^{-5}
12	~0.071233	4.6988×10^{-9}

where ε can be any extremely small positive value but not zero, and λ_G can be obtained by performing GA. Based on the experiments performed here, it was concluded that if σ_R equals $\sqrt{2}$ and $g=1$, then λ_R is approximately 0.567700. (see Table I).

2) Photoreceptor: An impulse response of a photoreceptor can be represented as a Difference of two Gaussians (DoG). In the retinal fovea, the DoG can be described as a Gaussian function, as shown below, in most cases [4], [5], [8]

$$g_{\sigma_R}(\mathbf{k}) = \frac{1}{\sqrt{2\pi\sigma_R^2}} e^{-\|\mathbf{k}\|^2/2\sigma_R^2}. \tag{41}$$

As mentioned in [8], parameter σ_R represents the standard deviation with a range from 1.5 to 12 (csp).

In the proposed approach, a CNN-based Gaussian-like operator is used for the simulation of the Gaussian function. That is

$$\mathrm{CNN}_{\mathrm{Gaussian},\lambda_R}(\delta(\mathbf{k})) \approx g_{\sigma_R}(\mathbf{k}) \tag{42}$$

where λ_R indicates the diffusion level of the Gaussian-like function. The next question is how to obtain the parameter λ_R and make the final state of the CNN approximate that shown in (41). To obtain the corresponding value λ_R, genetic algorithm (GA) is used again. Based on the results of the experiments, it was concluded that if σ_R equals 1.5, λ_R is approximately 0.536040, and if σ_R equals 12, then λ_R is approximately 0.071233 (see Table I).

Clearly, the RF of the photoreceptor is used to determine the average intensity of a specific area of a visual signal. Generally, it acts like a low-pass filter. The output of the filter, described in (42), is known as the first-order feature.

3) Horizontal Cell: Equation (38) implies that a horizontal cell can be implemented by the following:

$$h_{RH}(\mathbf{k}) = \frac{1}{b}\cdot(\delta(\mathbf{k}) - h_{RB}(\mathbf{k})). \tag{43}$$

Thus, estimating $h_{RB}(\mathbf{k})$ results in the realization of a horizontal cell $h_{RH}(\mathbf{k})$, if and only if the inverse operator of $h_R(\mathbf{k})$ exists. Thus, $h_{RB}(\mathbf{k})$ can be obtained as

$$h_{RB}(\mathbf{k}) = \frac{1}{g}\cdot h_G(\mathbf{k}) \otimes h_R^{-1}(\mathbf{k}). \tag{44}$$

Above it is assumed that the subject system is a monochromatic system. This means that the input of the bipolar and horizontal cells derives from the same set of the photoreceptors. If the inputs of the two types of cells do not derive from the same set of photoreceptors, then the RF of the horizontal cell needs to be known. Assume the input of a horizontal cell derives from photoreceptor system $h_{R'}(\mathbf{k})$ which is illustrated in Fig. 5(c), then based on (43), $h_{R'H}(\mathbf{k})$ can be obtained as follows:

$$h_{R'H}(\mathbf{k}) = \frac{1}{b}\cdot h_{R'}^{-1}(\mathbf{k}) \otimes \left(h_R(\mathbf{k}) - \frac{1}{g}\cdot h_G(\mathbf{k})\right). \tag{45}$$

Based on CNN, the horizontal cell $h_H(\mathbf{k})$ can be implemented by

$$h_H(\mathbf{k}) = \frac{1}{b}\cdot\Bigg(\delta(\mathbf{k}) - \mathrm{CNN}_{\mathrm{Laplace},\varepsilon} \times\left(\frac{1}{g}\cdot\mathrm{CNN}_{\mathrm{Gaussian},\lambda_G}\left(\mathrm{CNN}^{-1}_{\mathrm{Gaussian},\lambda_R}(\mathbf{k})\right)\right)\Bigg). \tag{46}$$

Horizontal cell determines the difference between the output signal of the photoreceptors in the center and the surroundings of a RF. This kind of feature is termed the second-order feature. Meanwhile, the final feature involves the determination of the parameters b and g. From a biological perspective, value b represents the related weights of the input signals of the horizontal cells, while g denotes the related weight of the ganglion. Unfortunately the values are unknown. However, considering the cooperation among the photoreceptor, horizontal cell, bipolar cell, and ganglion, it can be concluded that if an input is nothing but gray, which means there is no stimulation, then the output of the ganglions should be zero. This fact can help us to determine the values of b and g in a specific environment.

Finally, this study concludes that the photoreceptors, horizontal cells, and ganglions can be simulated as follows:

$$\mathrm{CNN}_{\mathrm{Photoreceptor},\lambda_R}(u(\mathbf{k})) = \mathrm{CNN}_{\mathrm{Gaussian},\lambda_R}(u(\mathbf{k})) \tag{47}$$

$$\mathrm{CNN}_{\mathrm{Horizontal},\varepsilon,b,g,\lambda_R,\lambda_G}(u(\mathbf{k})) = \frac{1}{b}\cdot\Bigg(\delta(\mathbf{k}) - \mathrm{CNN}_{\mathrm{Laplace},\varepsilon}\Bigg(\frac{1}{g}\cdot\mathrm{CNN}_{\mathrm{Gaussian},\lambda_G} \times\left(\mathrm{CNN}^{-1}_{\mathrm{Gaussian},\lambda_R}(u(\mathbf{k}))\right)\Bigg)\Bigg) \tag{48}$$

and

$$\mathrm{CNN}_{C-\mathrm{Ganglion},\varepsilon,b,g,\lambda_{R_u},\lambda_{R_v},I_G}(u(\mathbf{k}),v(\mathbf{k})) = \mathrm{CNN}_{\mathrm{Photoreceptor},\lambda_{R_u}}(u(\mathbf{k})) - \mathrm{CNN}_{\mathrm{Horizontal},\varepsilon,b,g,\lambda_R,\lambda_G}(v(\mathbf{k})). \tag{49}$$

Notably, $u(\mathbf{k})$ and $v(\mathbf{k})$ are the inputs of the photoreceptors. For a monochromatic system, the ganglion function is

$$\mathrm{CNN}_{M-\mathrm{Ganglion},\varepsilon,b,g,\lambda_{R_u},\lambda_G}(u(\mathbf{k})) = \Bigg(\mathrm{CNN}_{\mathrm{Photoreceptor},\lambda_{R_u}}(u(\mathbf{k})) - \mathrm{CNN}_{\mathrm{Horizontal},\varepsilon,b,g,\lambda_{R_u},\lambda_G}(u(\mathbf{k}))\Bigg). \tag{50}$$

III. EXPERIMENTS

A. Biology Related Visual Response and Illumination

Figs. 6 and 7 illustrate the impulse response of a horizontal cell in the hCNN-based computer fovea model. Note that

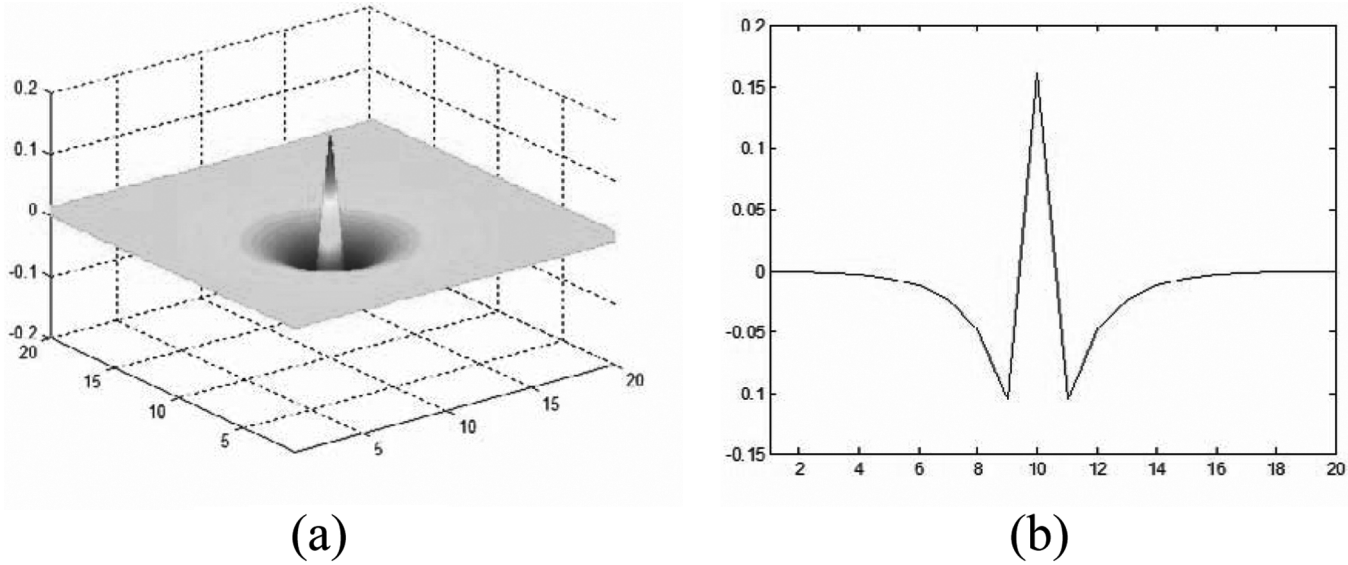

Fig. 6. Example of a center-on/surround-off RF, where, $\lambda_R = 0.53604$, $\lambda_G = 0.5677$, $\varepsilon = 0.01$ and $b = 0.75$.

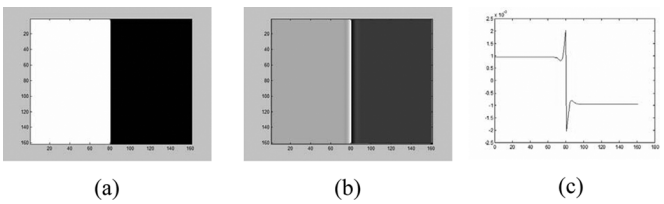

Fig. 7. Example of the model, where (a) is the input and (b) represents the output of the ganglions, while (c) shows the intensity of a section of (b). Notably, the behaviors of this model resembles that of the human vision visual system (see Fig. 3).

Fig. 6(a) can be compared with the well known RF structure (see Fig. 1). Notably, Fig. 7(b) resembles a common illumination in the human vision system.

Fig. 8 shows another example usign the proposed model, where the input is a natural image. Fig. 8(a) is the input, Fig. 8(b) is the output of horizontal cells, Fig. 8(c) is the output of the ganglions, and finally, Fig. 8(d) is the output of the rectification. Notably, to present the hexagonal structure, the resolution of the images in this example is reduced.

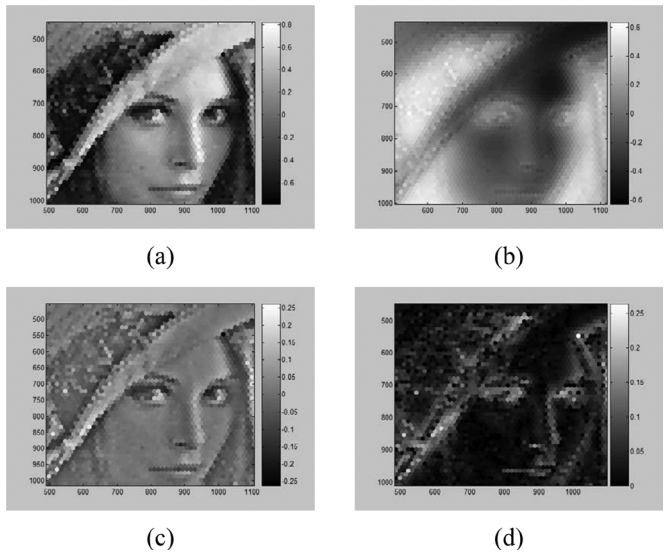

Fig. 8. Another example of the proposed model, where the input is a natural image. (a) Input. (b) Output of the horizontal cells. (c) Output of the ganglions. (d) Output following the rectification. Notably, to present the structure of the hexagonal structure, the resolution of the image is reduced in this example.

B. Simulation of a Retina and Central retinal vein occlusion (CRVO)

Color vision is quite an arbitrary experience, and thus a standard distribution of the sensitivity of the L-cone, the M-cone, and the S-cone cells in the human vision system is used for the simulation purpose in this study [see Fig. 9(a)], and mapped into an image frame. The data of the image frame is described using the specifications of a standard display device. The specifications include the spectral power distributions of the RGB primaries, and a transformation look-up table that describes the nonlinear relationship between the frame-buffer values in the image frame. The intensity of the light emitted by the each of the primaries on the display devices is labeled the display gamma curve (DGC). Fig. 9(b) and (c) shows these data.

Thus, a transform operator can be obtained as follows:

$$\begin{bmatrix} l(k) \\ m(k) \\ s(k) \end{bmatrix} = s \cdot T \cdot \begin{bmatrix} gR(k) \\ gG(k) \\ gB(k) \end{bmatrix} \tag{51}$$

where

$$T = C' \cdot D = \begin{bmatrix} 0.0209 & 0.0760 & 0.01126 \\ 0.0079 & 0.0764 & 0.0163 \\ 0.0009 & 0.0080 & 0.0766 \end{bmatrix}.$$

Here C denotes the normalized response of the L-cone, M-cone, and S-cone cells in the human vision system, and D represents the radiance data of red, green, and blue phosphor of the standard CRT. Notably, the input data $gR(\mathbf{k})$, $gG(\mathbf{k})$, and $gB(\mathbf{k})$ are adjusted using the GDC coefficient g, and s is a necessary

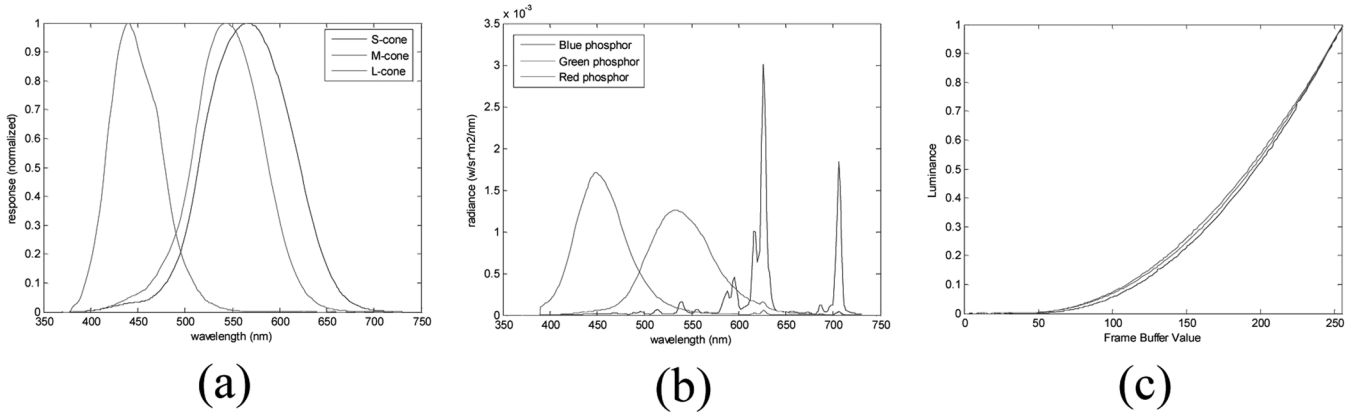

Fig. 9. (a) Corresponding responses of the L-cone, the M-cone, and the S-cone cells in the different wavelengths. (b) Spectral power distributions of the RGB primaries. (c) Transformation look-up table which describes nonlinear relationship between the frame-buffer values in the image data and the intensity of the light emitted by each of the primaries on the display, named the DGC.

scale value. The related data $u_R(\mathbf{k})$, $u_G(\mathbf{k})$, $u_B(\mathbf{k})$, and $u_Y(\mathbf{k})$ then can be obtained as follows:

$$\begin{aligned} u_R(\mathbf{k}) &= l(\mathbf{k}) \\ u_G(\mathbf{k}) &= m(\mathbf{k}) \\ u_B(\mathbf{k}) &= s(\mathbf{k}) \\ u_Y(\mathbf{k}) &= \frac{1}{2}(l(\mathbf{k}) + m(\mathbf{k})) \end{aligned} \tag{52}$$

where $l(\mathbf{k})$, $m(\mathbf{k})$, and $s(\mathbf{k})$ represent the related signals of the L-cone, M-cone, and S-cone cells.

To present the image, the experiments use CIE $-$ $L^*a^*b^*$ color space. The CIE$-L^*a^*b^*$ diagram is known as the psychometric color diagram. The colors of the diagram lie at right angles to one another in two directions, and the plane thus created is distributed at right angles to the achromatic axis. The resultant uniform color-space is of course based on the four psychological basic-colors of red, green, blue, and yellow—first described by Hering in his opponent-theory—which are now known to be transmitted directly to the brain.

In this simulation, the R, G, B, and Y channels can be selected as the inputs. Consequently, the input values of CIE $-$ $L^*a^*b^*$ can be obtained as follows:

$$\begin{aligned} L(\mathbf{k}) &= \max(u_R(\mathbf{k}), u_G(\mathbf{k}), u_B(\mathbf{k})) \\ a(\mathbf{k}) &= \mathrm{CNN}_{C-\mathrm{Ganglion},\varepsilon,b,g,\lambda_{R_u},\lambda_G} \\ &\quad \cdot (u_R(\mathbf{k}), u_G(\mathbf{k})) \\ \text{and } b(\mathbf{k}) &= \mathrm{CNN}_{C-\mathrm{Ganglion},\varepsilon,b,g,\lambda_{R_u},\lambda_G} \\ &\quad \cdot (u_B(\mathbf{k}), u_Y(\mathbf{k})). \end{aligned} \tag{53}$$

Based on the definition of CIE $-$ $L^*a^*b^*$, the color channels red, green, and blue can be obtained as follows:

$$\begin{aligned} l'(\mathbf{k}) &= \begin{cases} a(\mathbf{k}), & a(\mathbf{k}) > 0 \\ 0, & \text{otherwise} \end{cases} \\ m'(\mathbf{k}) &= \begin{cases} -a(\mathbf{k}), & a(\mathbf{k}) < 0 \\ 0, & \text{otherwise} \end{cases} \\ \text{and } s'(\mathbf{k}) &= \begin{cases} b(\mathbf{k}), & b(\mathbf{k}) > 0 \\ 0, & \text{otherwise.} \end{cases} \end{aligned} \tag{54}$$

(a) (b) (c)

Fig. 10. This study uses an RG and a BY channel as the input of the center-red-on/surround-green-off and center-blue-on/surround-yellow-off ganglions, and consequently the new red-to-green and blue-to-yellow chromatic aberrations are obtained. (a) Test image. (b) Reconstructed result. These new chromatic aberrations were used to reconstruct the image, and compare it with the original. The average PSNR is 32.2263 dB. (c) Simulation result of the CRVO.

Finally, the work of (51) and GDC coefficient g are reversed. Restated

$$\begin{bmatrix} g^{-1}R'(\mathbf{k}) \\ g^{-1}G'(\mathbf{k}) \\ g^{-1}B'(\mathbf{k}) \end{bmatrix} = s^{-1} \cdot T^{-1} \cdot \begin{bmatrix} l'(\mathbf{k}) \\ m'(\mathbf{k}) \\ s'(\mathbf{k}) \end{bmatrix} \tag{55}$$

where $R'(\mathbf{k})$, $G'(\mathbf{k})$, and $B'(\mathbf{k})$ are the final outputs.

On the other hand, the present experiment simulates a center-red-on/surround-green-off and a center-blue-on/surround-yellow-off ganglion. The new red-to-green and blue-to-yellow chromatic aberrations are thus obtained.

A result is shown in Fig. 10, where Fig. 10(a) denotes the input, and Fig. 10(b) represents the corresponding output. These new chromatic aberrations are used to reconstruct the image and compare it with the original one. The average peak signal-to-noise rate (PSNR) is 32.2263 dB.

CRVO is a well-known retinal disease. Because a retina needs a lot of oxygen to function, significant blood circulation is necessary. Normally, blood flows into the retina via the central retinal artery (CRA) and leaves via the central retinal vein (CRV). Both of these blood vessels enter the eye through the optic nerve. CRVO is caused by a blood clot in the CRV, which slows or stops blood flow out of the retina. Although initially blood may continue to enter the retina through the CRA, the

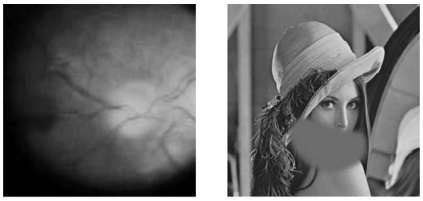

(a) (b)

Fig. 11. Case of a retinal injury and its visual response. (a) Retina CRVO. The vein on the left side of the fovea is clogged and results retinal injury. (b) The patient will "sense" a piece of gray in the area of the retina that has lost blood circulation.

(a) (b)

Fig. 12. Example of improvement in image sharpness. (a) Input. (b) Output. The images can be obtained at (http://cnn.cn.nctu.edu.tw/~chhuang/paper/hC-NNCFM/).

blockage ultimately stops blood circulation. As a result, blood and fluid are backed up, causing retinal injury and vision loss. Consequently, the brain thus becomes confused and the patient will "sense" a piece of gray in the area of the retina that has lost blood circulation (see Fig. 11).

A simulation result of CRVO is represented in Fig. 10(c). Human vision is a complex system, and cannot be comprehensively simulated. Even now, only some of the architecture of this system is known. However, some of the features of the present simulation closely resemble those of human vision system. First, the output of the simulator [Fig. 10(b)] closely resembles the input [Fig. 10(a)], even though the color channels are modified. This result implies that the human vision system cannot sense minor differences in color. Second, in the CRVO region, the stimulations of the cells in a specific region are stopped, and the CRVO region can be seen to be gray. This result demonstrates that if there is no signal in a given region, the human vision system will sense a piece of gray in the scene. These conclusions correlate with the results of medical investigations.

C. Image Sharpness Improvement

In the human vision system, the second-order features can provide [the related difference of light intensity between the cells. This is why the human vision system can reliably identify different textures under variable light conditions. On the other hand, a kind of amacrine cell, named biplexiform ganglion cell, is directly connected to the photoreceptors. The biplexform ganglion cell are depolarising in response to increases in photon catch and as a result, it can provide information regarding ambient light level, which is useful for controlling pupil diameter and diurnal body rhythm. Thus, the responses of the connected ganglion can be used to implement the improvement in sharpness. For the luminance channel of CIE$-L^*a^*b^*$, the following equation can be applied:

$$\begin{aligned} L'(\mathbf{k}) = {} & L(\mathbf{k}) + \alpha_1 \cdot \mathrm{CNN}_{M-\mathrm{Ganglion},\varepsilon_1,b_1,g_1,\lambda_{1,R_u},\lambda_{1,G}} \\ & \cdot (L(\mathbf{k})) + \cdots + \alpha_n \\ & \cdot \mathrm{CNN}_{M-\mathrm{Ganglion},\varepsilon_n,b_n,g_n,\lambda_{n,R_u},\lambda_{n,G}} (L(\mathbf{k})) \end{aligned} \quad (56)$$

where $\alpha_1, \alpha_2, \ldots, \alpha_n$ represent the function of the biplexiforms. Fig. 12 shows an example of image sharpness, where Fig. 12(a) is the original input, and Fig. 12(b) is the output. In fact, this algorithm matches the conclusions of Kotera. Korera previously proposed a sharpness improvement algorithm based on the detection of adaptive edges [25].

D. Color Constancy

According to the gray world hypothesis, in the absence of other colors the world is perceived as gray , [26]. Based on this assumption, the proposed model can be used to estimate the shift in the light. Furthermore, light shifting can be removed via this model.

The stimulation outputs of a horizontal cell are fed back to the connected photoreceptors to reduce the influence of photoreceptors on the bipolar cells. This lateral inhibition results in activation of any one photoreceptor reducing that of surrounding photoreceptors. In some cases, the central and peripheral photoreceptors react to same kind of the stimulations and thus exert a mutually depressive effect [1]. A monochromatic system provides an example. Thus, this study concludes that a special case of central/surround structure stands as follows:

$$\begin{aligned} a'(\mathbf{k}) = {} & \alpha_a \cdot \Big(a(\mathbf{k}) - \mathrm{CNN}_{M-\mathrm{Ganglion},\varepsilon,b,g,\lambda_R} \\ & \cdot (a(\mathbf{k})) \Big) + \beta_a \\ b'(\mathbf{k}) = {} & \alpha_b \cdot \Big(b(\mathbf{k}) - \mathrm{CNN}_{M-\mathrm{Ganglion},\varepsilon,b,g,\lambda_R} \\ & \cdot (b(\mathbf{k})) \Big) + \beta_b \end{aligned} \quad (57)$$

where ε is a small value, $b = 0$, $g = 1$, $\lambda_R = 0.6$, α_a and α_b are the related scale, and β_a and β_b represent the definition of "gray". Generally, the α and β are unnecessary. However, in some situations the related environment of the input image is quite extreme and thus the range of the color space is limited. In such cases, α and β are required to restore the image. Fig. 13 shows an example and the results.

E. Video Auto Adjustment and Enhancement

Since the model parameters are obtained from the input image, the computer fovea model can be used to perform adaptive adjustment and enhancement of sequential images (i.e., video). This experiment applied the proposed visual information from the enhancing algorithm for the each image

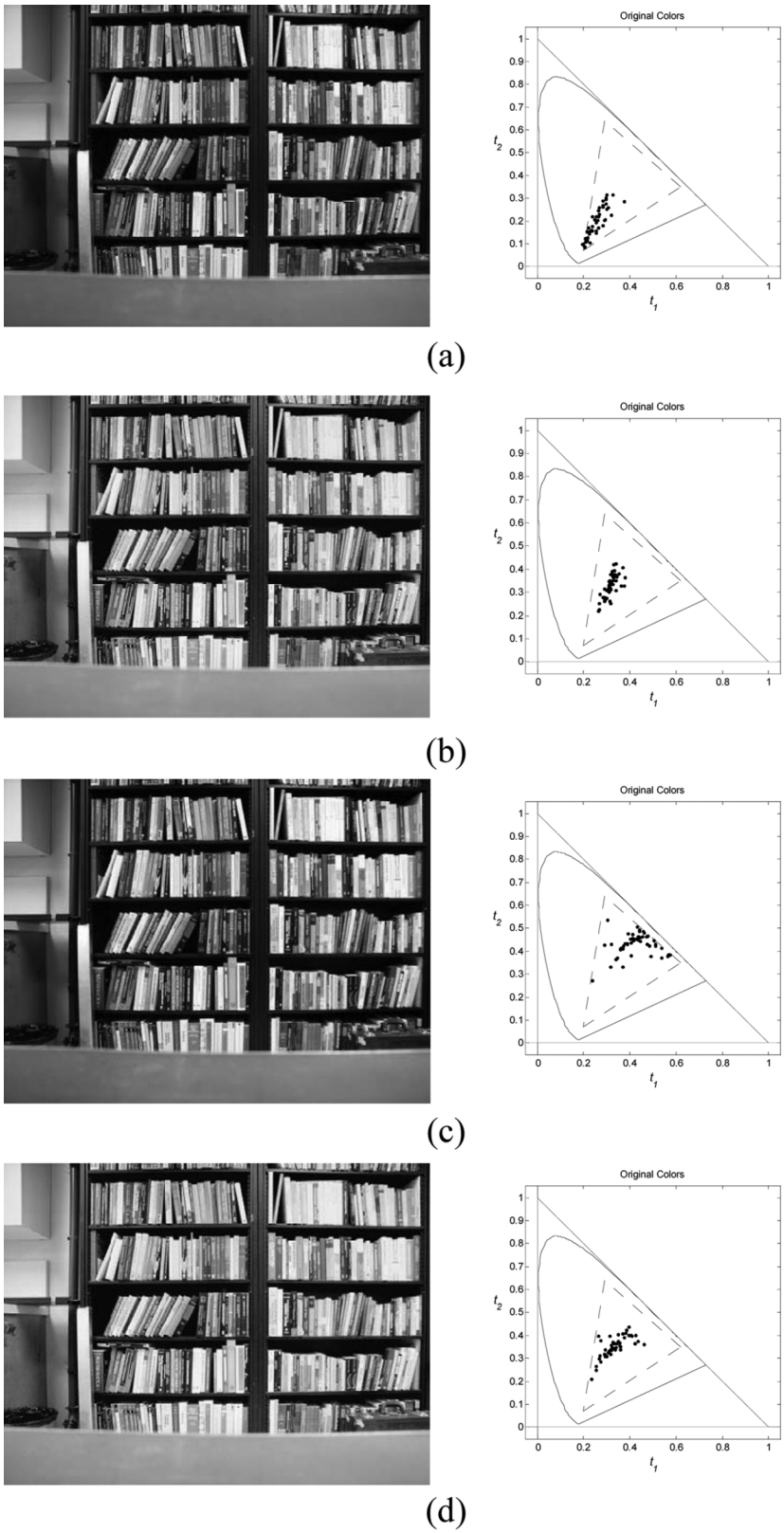

Fig. 13. Two results of the proposed image color constancy algorithm. First, a photo is taken under a blue light condition. The photo is shown in (a), and the reconstructed result is shown in (b). Next, a photo is taken of the same scene under yellow light condition, as shown in (c), and the reconstructed result is shown in (d). The chromatic diagrams are shown to the side of the images. The images can be obtained at (http://cnn.cn.nctu.edu.tw/~chhuang/paper/hCNNCFM/).

in the videos. Fig. 14 shows the experiment results, where Fig. 14(a) and (c) are the inputs, while (b) and (d) are the video outputs. Notably, the algorithm is adaptively adjusted during processing.

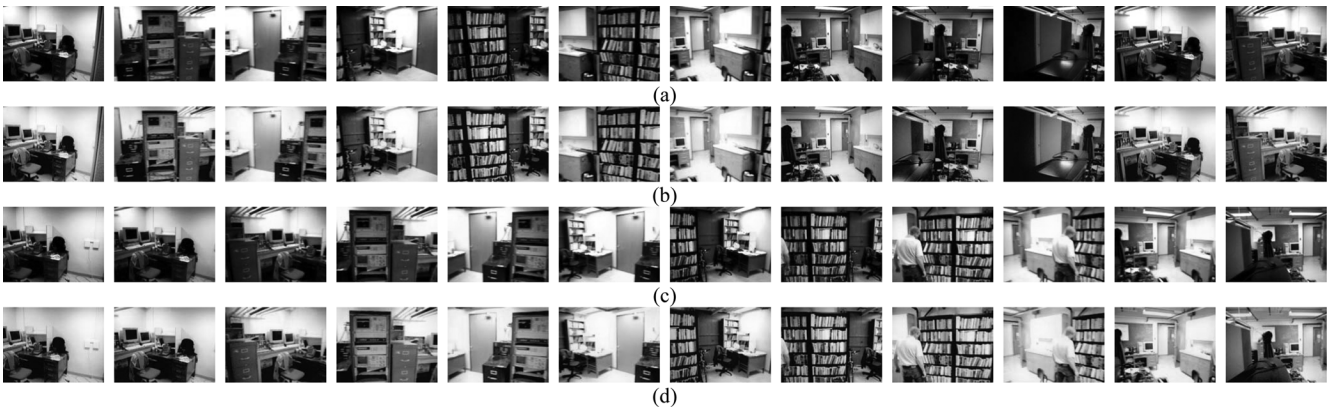

Fig. 14. Two experimental results of the integrated video auto adjustment and enhancing algorithm, where(a), (c) are the input videos, (c) and (d) are the reconstructed outputs. The full video can be obtained at (http://cnn.cn.nctu.edu.tw/~chhuang/paper/hCNNCFM/).

IV. Conclusion

This work studied the possibilities for implementing an hCNN-based computer fovea model. Although the details of the fovea, retina, and even the whole of the human vision system remain unknown, based on some results of previous researches on both biology and digital image processing, the fovea model can be roughly realized, and consequently some possible applications can be fulfilled. However, some issues remain open to question. For example, this experiment examines 2 or 3 types of ganglions. In fact, over 20 different structures of ganglions have already been identified. Thus, it is interesting to consider the relationships among these different types of implementations, particularly in cases where the response of a ganglion is related to the time domain. On the other hand, the results of the video processing may differ from those in the proposed model. Roska and Bálya *et al.* discussed the parallel structure of the mammalian retina and its implementation in CNN [6]. Their study indicated demonstrated the complexity of the retina. Studying the relationship between the structure of the retina and possible applications for image processing offers one of the most interesting topics for future research.

References

[1] D. H. Hubel, *Eye, Brain, and Vision*. New York: Scienceific American, 1988.
[2] D. H. Hubel and T. N. Wiesel, "Receptive fields, binocular interaction, and functional architecture in the cat's visual cortex," *J. Physiol. (Lond.)*, vol. 160, pp. 106–154, 1962.
[3] J. I. Yellot, "Spectral consequences of photoreceptor sampling in the rhesus retina," *Science*, vol. 221, pp. 382–385, 1983.
[4] S. Shah and M. D. Levine, "Visual information processing in primate cone pathways— II: Experiments," *IEEE Trans. Syst., Man, Cybern. B, Cybern.*, vol. 26, no. 2, pp. 275–289, Feb. 1996.
[5] J. Thiem and G. Hartmann, "Biology-inspired design of digital gabor filters upon a hexagonal sampling scheme," in *Proc. Int. Conf. Pattern Recogn. (ICPR'00)*, Barcelona, Spain, 2000.
[6] D. Bálya, B. Roska, T. Roska, and F. S. Werblin, "A CNN framework for modeling parallel processing in a mammalian retina," *Int. J. Circuit Theory Appl.*, vol. 30, pp. 363–393, 2002.
[7] B. Roska and F. S. Werblin, "Vertical interactions accross ten paralel, stacked representations in the mammalian retina," *Nature*, vol. 410, pp. 583–587, 2001.
[8] S. Shah and M. D. Levine, "Visual information processing in primate cone pathways—Part I: A model," *IEEE Trans. Syst., Man, Cybern. B, Cybern.*, vol. 26, no. 2, pp. 259–274, Feb. 1996.
[9] A. K. Jain, "Unsupervised texture segmentation using gabor filters," *Pattern Recogn.*, vol. 24, pp. 1167–1186, 1991.
[10] A. Jacobs and F. S. Werblin, "Spatiotemporal patterns at the retinal output," *J. Neurophysiol.*, vol. 80, pp. 447–451, 1998.
[11] B. K. P. Horn, "Determining lightness from an image," *Comput. Graphics Image Process.*, pp. 277–299, 1974.
[12] C. H. Huang and C. T. Lin, "Cellular neural networks for hexagonal image processing," in *Proc. Int. Workshop Cellular Neural Networks Their Applications,* , Hsinchu, Taiwan, R.O.C., 2005.
[13] H. Kobayashi, J. L. White, and A. A. Abidi, "An active resister network for Gaussian filtering of images," *IEEE J. Solid-State Circuits*, vol. 26, no. 3, pp. 738–748, Jun. 1991.
[14] I. Her, "A symmetrical coordinate frame on the hexagonal grid for computer graphics and vision," *ASME J. Mech. Design*, vol. 115, pp. 447–449, 1993.
[15] S. B. M. Bell, F. C. Holroyd, and D. C. Mason, "A digital grometry for hexagonal pixels," *Image Vision Comput.*, vol. 7, pp. 194–204, 1989.
[16] L. O. Chua and L. Yang, "Cellular neural networks: Theory," *IEEE Trans. Circuits Syst.*, vol. 35, no. 12, pp. 1257–1272, Dec. 1988.
[17] ——, "Cellular neural networks: Applications," *IEEE Trans. Circuits Syst.*, vol. 35, no. 12, pp. 1273–1290, Dec. 1988.
[18] G. Seiler and J. A. Nossek, "Symmetry properties of cellular neural networks on square and hexagonal grids," in *Proc. Int. Workshop Cellular Neural Networks Their Applications,* , 1992, pp. 258–263.
[19] L. Middleton and J. Sivaswamy, "Framework for partical hexagonal-image processing," *J. Electron. Imag.*, vol. 11, pp. 104–114, Jan. 2002.
[20] K. R. Crounse and L. O. Chua, "Methods for image processing and pattern formation in cellular neural networks," *IEEE Trans. Circuits Syst. I, Fundam. Theory Appl.*, vol. 42, no. 4, pp. 583–601, Apr. 1995.
[21] L. Middleton, J. Sivaswamy, and G. Coghill, "The FFT in a hexagonal-image processing framework," in *Proc. New Zealand Image Vision Comput. Conf.*, Dunedin, New Zealand, 2001.
[22] B. E. Shi, "Gabor-type filtering in space and time with cellular neural networks," *IEEE Trans. Circuits Syst. I, Fundam. Theory Appl.*, vol. 45, no. 1, pp. 121–132, Jan. 1998.
[23] H. Steklis and J. Erwin, "The primate retina," *Compar. Primate Biol., Neurosci.*, vol. 4, pp. 203–278, 1988.
[24] S. Shah and M. D. Levine, "The primate retina: A biological summary," Ph.D. dissertation, Center for Intelligent Machines, , McGill University, Montreal, QC, Canada, 1992.
[25] H. Kotera, Y. Yamada, and K. Shimo, "Sharpness improvement adaptive to edge strength of color images," in *Proc. Color Imaging Conf. 2000*, Scottsdale, AZ, 2000.
[26] G. Buchsbum, "A spatial processor model for object colour perception," *J. Franklin Inst.*, vol. 310, pp. 337–350, 1980.

Chao-Hui Huang (S'05) received the M.S. degree in computer science and information engineering from Chung-Hua University (CHU), Taiwan, R.O.C., in 2001. He is currently working toward the Ph.D. degree at National Chiao-Tung University (NCTU), Taiwan, R.O.C.

His research interests are in the areas of artificial intelligence, soft computing, and bio-inspired information system.

Chin-Teng Lin (F'05) received the B.S. degree from National Chiao-Tung University (NCTU), Taiwan, R.O.C., in 1986, and the Ph.D. degrees in electrical engineering from Purdue University, West Lafayette, IN, in 1992.

He is currently the Chair Professor of Electrical and Computer Engineering, Dean of Computer Science College, and Director of Brain Research Center at NCTU. His current research interests are fuzzy neural networks, cellular neural networks, smart vision systems, and computational neuroscience. He is the coauthor of the book *Neural Fuzzy Systems—A Neuro-Fuzzy Synergism to Intelligent Systems* (Prentice-Hall, 1996), and the author of *Neural Fuzzy Control Systems with Structure and Parameter Learning* (World Scientific, 1994).

Dr. Lin is an IEEE Fellow for his contributions to biologically inspired information systems. He currently serves on the Board of Governors at IEEE Circuits and Systems (CAS) Society (2005–2008), and served for the IEEE Systems, Man, Cybernetics (SMC) Society in 2003–2005. He was the Distinguished Lecturer of IEEE CAS Society from 2003 to 2005. He was Special Session Co-Chair of ISCAS 2006 in Greece, and the Program Co-Chair of IEEE Proc. Int. Conf. SMC 2006 in Taiwan. He has been the President of Asia Pacific Neural Network Assembly since 2004.